

Multiobjective Optimization for Electronic Circuit Design in Time and Frequency Domains

Josef DOBEŠ¹, Jan MÍCHAL², Viera BIOLKOVÁ³

¹Department of Radio Engineering, Czech Technical University in Prague, Technická 2, 166 27 Praha 6, Czech Republic

²Division of Integrated Circuit Design, CertiCon Corporation, Václavská 12, 120 00 Praha 2, Czech Republic

³Department of Radio Electronics, Brno University of Technology, Purkyňova 118, 612 00 Brno, Czech Republic

dobes@fel.cvut.cz, michal@fel.cvut.cz, biolkova@feec.vutbr.cz

Abstract. The multiobjective optimization provides an extraordinary opportunity for the finest design of electronic circuits because it allows to mathematically balance contradictory requirements together with possible constraints. In this paper, an original and substantial improvement of an existing method for the multiobjective optimization known as GAM (Goal Attainment Method) is suggested. In our proposal, the GAM algorithm itself is combined with a procedure that automatically provides a set of parameters – weights, coordinates of the reference point – for which the method generates noninferior solutions uniformly spread over an appropriately selected part of the Pareto front. Moreover, the resulting set of obtained solutions is then presented in a suitable graphic form so that the solution representing the most satisfactory tradeoff can be easily chosen by the designer. Our system generates various types of plots that conveniently characterize results of up to four-dimensional problems. Technically, the procedures of the multiobjective optimization were created as a software add-on to the CIA (Circuit Interactive Analyzer) program. This way enabled us to utilize many powerful features of this program, including the sensitivity analyses in time and frequency domains. As a result, the system is also able to perform the multiobjective optimization in the time domain and even highly nonlinear circuits can be significantly improved by our program. As a demonstration of this feature, a multiobjective optimization of a C-class power amplifier in the time domain is thoroughly described in the paper. Further, a four-dimensional optimization of a video amplifier is demonstrated with an original graphic representation of the Pareto front, and also some comparison with the weighting method is done. As an example of improving noise properties, a multiobjective optimization of a low-noise amplifier is performed, and the results in the frequency domain are shown. Finally, a necessity of a use of metaheuristic methods at least with a combination with the classical ones is demonstrated.

Keywords

Multiobjective optimization, Pareto front, Pareto optimal set, noninferior solutions, goal attainment method, metaheuristics, simulated annealing, hybrid methods.

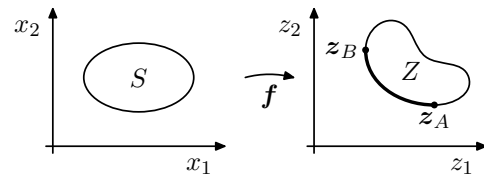


Fig. 1. Feasible region (S), feasible objective region (Z), and Pareto front.

1. Introduction

The process of electronic circuit design usually strongly relies on the use of computers. One class of methods for circuit design not only uses them as a circuit simulation tool, but also uses numerical optimization algorithms as a means of determining parameter values in order to bring the designed circuit as close as possible to some prescribed behavior or a set of characteristics. Multiobjective optimization solves the situations in circuit design where there are two or more possibly contradictory requirements on a circuit and thus a suitable tradeoff needs to be found. Such a tradeoff solution should best belong to a set of noninferior solutions, also called Pareto optimal set or Pareto front.

1.1 Multiobjective Optimization Problem

In practical designs, there are often multiple mutually contradicting requirements on the designed circuit. In such cases, our aim is to solve the corresponding *multiobjective optimization problem*. This can be formally written as

$$\underset{\mathbf{x} \in S}{\text{minimize}} \quad \{f_1(\mathbf{x}), f_2(\mathbf{x}), \dots, f_k(\mathbf{x})\} \quad (1)$$

where we have k objective functions $f_i: \mathbb{R}^n \rightarrow \mathbb{R}$, $k \geq 2$. As in the case of the singleobjective optimization problem, the decision vectors $\mathbf{x} = (x_1, x_2, \dots, x_n)^T$ belong to the (nonempty) feasible region S , $S \subseteq \mathbb{R}^n$, which can also be defined by a number of equality constraints, inequality constraints, and/or bounds on the decision variables x_i . The vector of objective functions is denoted by $\mathbf{f}(\mathbf{x}) =$

$[f_1(\mathbf{x}), f_2(\mathbf{x}), \dots, f_k(\mathbf{x})]^T$ and the image of the feasible region, also called the *feasible objective region* [1, 5], is denoted by $Z = \mathbf{f}(S)$, $Z \subseteq \mathbb{R}^k$. The elements of Z are called *objective vectors* and are denoted by $\mathbf{f}(\mathbf{x})$ or $\mathbf{z} = [z_1, z_2, \dots, z_k]^T$, where $z_i = f_i(\mathbf{x})$ for all $i = 1, 2, \dots, k$ are *objective values*. The geometrical representation of both sets S and Z and of the mapping $\mathbf{f}(\mathbf{x})$ between them can easily be illustrated on a two-dimensional case, as shown in Fig. 1 for $n = 2$ and $k = 2$.

1.2 Pareto Optimality

The word “minimize” in (1) means that we want to minimize all the objective functions simultaneously. However, because of the contradiction between the objective functions, it is not possible to find a single solution that would be optimal for all the objectives simultaneously. The concept of *noninferiority* also called *Pareto optimality* must be used to characterize the objective vectors. A noninferior solution is the one in which an improvement in one objective requires a deterioration of another. The set of all noninferior solutions is also called the *Pareto front*. In Fig. 1 it is marked by the thick curve segment between points \mathbf{z}_A and \mathbf{z}_B .

By solving the problem (1) we understand obtaining a sufficient number of noninferior solutions covering parts of the Pareto front that are of interest to the designer. This will allow him or her to fully understand the available trade-offs and to take a qualified decision based on this knowledge.

1.3 Ranges of the Pareto Front

For normalizing purposes we may need to know the minimum and maximum values of the individual objectives achieved over the Pareto Front. We will assume that individual objective functions $z_i = f_i(\mathbf{x})$ are bounded over the feasible region S .

Ideal objective vector [1, 5] $\mathbf{z}^* = [z_1^*, z_2^*, \dots, z_k^*]$ is the objective vector independently minimizing each objective function:

$$\mathbf{z}^* = \left[\min_{\mathbf{x} \in S} f_1(\mathbf{x}), \min_{\mathbf{x} \in S} f_2(\mathbf{x}), \dots, \min_{\mathbf{x} \in S} f_k(\mathbf{x}) \right]. \quad (2)$$

It can easily be seen that if the ideal objective vector is feasible ($\mathbf{z}^* \in Z$), it is a solution of the multiobjective optimization problem and the Pareto front is reduced to it. But even in the usual cases when ideal objective vector is not feasible, it can still be considered a useful reference point.

Maximum objective function values achieved over the Pareto front are represented by a *nadir objective vector* [1, 5]. Because such maxima are difficult to find, an approximate nadir vector \mathbf{z}^{nad} is instead defined as

$$\mathbf{z}^{\text{nad}} = \left[\max_i(z_i^*)_1, \dots, \max_i(z_i^*)_k \right], \quad (3)$$

i.e., as the vector of the largest respective components $(z_i^*)_j$

found in all k ideal objective vectors. Nadir vector may and may not be feasible.

1.4 A Posteriori Methods

A posteriori methods can be thought of as methods for generating Pareto optimal solutions. After the Pareto front (or a part of it) has been generated, it is presented to the decision maker, who selects the most preferred among the alternatives. The inconvenience here is that the generation process is usually computationally expensive and sometimes difficult. It may be hard for the decision maker to select from a large set of alternatives, especially with higher numbers of objective functions. Another important question is how to present or display the alternatives to the decision maker in an effective way.

1.4.1 Weighting Method

In the weighting method, the idea is to associate each objective function with a weighting coefficient and minimize the weighted sum of the objectives. We suppose that the weighting coefficients w_i are real numbers such that $w_i \geq 0$ for all $i = 1, \dots, k$. It is also usually supposed the weights are normalized so that $\sum_{i=1}^k w_i = 1$. The multiobjective optimization problem is then modified into the following problem, to be called a *weighting problem* [1–4]:

$$\text{minimize}_{\mathbf{x} \in S} \sum_{i=1}^k w_i f_i(\mathbf{x}). \quad (4)$$

It can be shown that the solution of the weighting method is always Pareto optimal if the weighting coefficients are all positive or if the solution is unique [1, 3].

The weakness of the weighting method is that not all of the Pareto optimal solutions can be found unless the problem is convex. This feature can be relaxed to some extent by convexifying the nonconvex Pareto front by raising the objective functions to a high enough power under certain assumptions.

Geometrical representations of the problems characterized the weighting method are shown in Figs. 2 and 3.

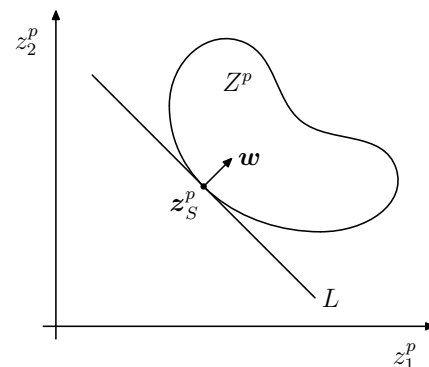


Fig. 2. Geometrical representation of weighting method.

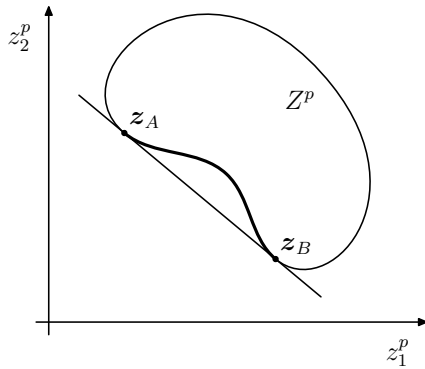


Fig. 3. Nonconvex feasible objective region.

Another weakness of the weighting method is the fact that it may be difficult to control the location of found solutions by the weighting coefficients.

1.4.2 ϵ -Constraint Method

In the ϵ -constraint method [2, 4], one of the objective functions is selected to be optimized and all the other objective functions are converted into constraints by setting an upper bound to them. The problem to be solved is now of the form

$$\begin{aligned} & \underset{\mathbf{x} \in S'}{\text{minimize}} && f_\ell(\mathbf{x}) \\ & S' = \{\mathbf{x} \mid \mathbf{x} \in S, f_j(\mathbf{x}) \leq \epsilon_j \text{ for all } j = 1, \dots, k, j \neq \ell\} \end{aligned} \quad (5)$$

where $\ell \in \{1, \dots, k\}$. Problem (5) is called an ϵ -constraint problem.

It can be proved that it is possible to find every Pareto optimal solution of any multiobjective optimization problem by the ϵ -constraint method (regardless of the convexity of the problem) [5].

To ensure that a solution produced by the ϵ -constraint method is Pareto optimal, we have to either solve k different problems or make sure that the obtained solution is unique. In general, uniqueness is not necessarily easy to verify. However, if for example, the problem is convex and the function f_ℓ to be minimized is strictly convex, we know that the solution is unique without further checking.

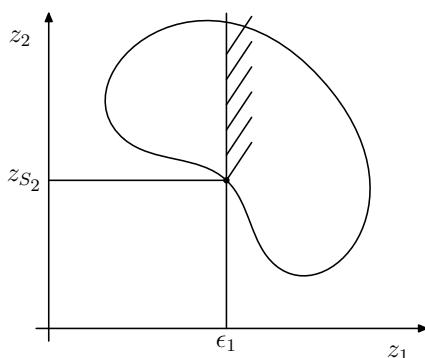


Fig. 4. Geometrical representation of ϵ -constraint method.

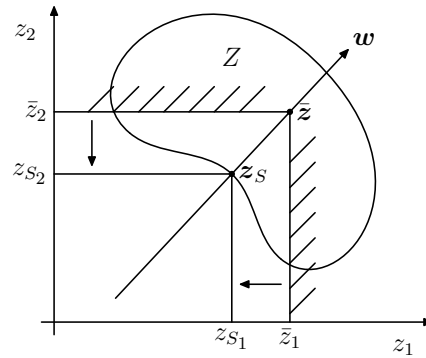


Fig. 5. Geometrical representation of GAM.

1.4.3 Goal Attainment Method

Typically used approaches to the multiobjective optimization are either a method based on a weighted sum or optimization of a single objective function while the others serve as constraints (here shown as ϵ -constraint method) [1, 5]. The goal attainment method [3, 6–8] provides a better control over obtained solutions. It is defined as a scalar constrained optimization problem of the form

$$\begin{aligned} & \underset{\gamma \in \mathbb{R}, \mathbf{x} \in S}{\text{minimize}} && \gamma \\ & \text{subject to} && f_i(\mathbf{x}) - w_i \gamma \leq \bar{z}_i, \\ & && i = 1, \dots, k, \end{aligned} \quad (6)$$

where f_i are the k objective functions to be minimized (design goals), S is the set of acceptable solutions (the feasible region), \bar{z}_i are predefined reference goal values associated with the objective functions f_i , $w_i \in \mathbb{R}$ are predefined weighting coefficients, and γ is an auxiliary variable making the new single objective function. The method requires $2k$ input parameters, but only uses $2k - 1$ degrees of freedom as shown in Fig. 5. Any solution of this optimization problem is noninferior. Its location on the Pareto front can be controlled by the weighting vector w and/or by the reference vector \bar{z} .

2. Semiautomatic A Posteriori Method

The goal is to arrange a reliable general-purpose multiobjective optimization tool that could be used in circuit design.

Requirements on the multiobjective optimization method will include:

- Arbitrary number of objectives,
- arbitrary number of inequality constraints (but no need for equality constraints),
- provisions for maximizing some functions while minimizing others,
- possibility of non-differentiable objectives,
- automatic generation of Pareto optimal solutions,

- automatic determining of what the covered part of the whole Pareto front will be,
- even density of coverage of selected part of the Pareto front,
- possibility of monitoring and user interference during computation run,
- support for graphical presentation of the solutions.

These requirements clearly suggest the use of an a posteriori method or a method of another class converted into an a posteriori method to be able to automatically generate Pareto optimal solutions.

The authors' choice is the Goal Attainment Method (GAM), which is also one of the Achievement Scalarizing Function approaches and a variety of Goal Programming [1].

Its advantages as opposed to Weighted Method or Method of Weighted Metrics [1] are that all Pareto optimal solutions are accessible even for non-convex problems and that it works for both feasible as well as infeasible reference points. The need for a subroutine for constrained optimization could be seen as a disadvantage, but we want to be able to work with constraints, anyhow.

There are two possible ways of controlling the location of the Pareto optimal solutions found by GAM: either (a) by the choice of the reference point or (b) by the choice of the weighting vector (or (c) a combination of both). Our approach uses (a) because this seems to have a better chance of even coverage of the Pareto front.

Here is the implemented equivalent form of the GAM, also with the used normalization:

$$\underset{\mathbf{x} \in S}{\text{minimize}} \quad \max_{i=1, \dots, k} \frac{f_i(\mathbf{x}) - \bar{z}_i}{z_i^{\text{nad}} - z_i^*}. \quad (7)$$

Note that this very formula works for both the minimized as well as maximized objective functions: for the maximized ones we have $z_i^{\text{nad}} - z_i^* < 0$ and the denominator thus automatically provides the correct sign. Also, as a result of the choice (a) mentioned above, there are no explicit weighting coefficients w_i used in (6). Note that the missing weighting coefficients in (7) which are a result of the choice (a) above also exclude the possibility to introduce hard constraints simply by setting the particular weight to zero, but this really poses no practical limitation in our implementation as any goal can easily be switched to directly play the role of an objective, a constraint, or even both of them simultaneously.

Now let us consider the choice of a set A in the k dimensional objective space from which the reference points are taken. We will call it the *reference set*.

It should not be too far away from the Pareto front (in Euclidian sense) so that it is not too complicated for the user

to predict where the corresponding Pareto optimal solution will be from the knowledge of the reference point.

If the feasible objective set is bounded, the Pareto front P will usually be a subset of the k -dimensional interval $B = \prod_{i=1}^k [z_i^*, z_i^{\text{nad}}]$, where the product operator represents the Cartesian product.

We could put $A = B$ and simply randomly generate the coordinates from the intervals $[z_i^*, z_i^{\text{nad}}]$. However, this approach would lead to many reference points that have no projection on the Pareto front. Such points could still provide Pareto optimal solutions but those would be concentrated along the border of Pareto front and not evenly spread over the interior. Also many points would be quite far from the Pareto front.

Therefore, we try to limit the size of the set A and select it such that it is likely to be not very far from Pareto front.

One such a choice of the reference set A , that has actually been implemented in the proposed method, is the k -dimensional convex body with k vertices (segment of straight line, triangle, tetrahedron, etc.) whose vertices are composed of one component of the ideal vector z_i^* and the rest are corresponding components of the nadir vector z^{nad} :

$$z_i^{\text{vert}} = [z_1^{\text{nad}}, \dots, z_{l-1}^{\text{nad}}, z_l^*, z_{l+1}^{\text{nad}}, \dots, z_k^{\text{nad}}]^T \quad \forall l = 1, \dots, k. \quad (8)$$

This set A is randomly sampled with the uniform distribution all over its $(k - 1)$ -dimensional volume. This is done with the intent to uniformly cover the corresponding part of the Pareto front. Fig. 6 illustrates the location of this reference set in the two- and three-dimensional objective space.

The random generation of reference points belonging to A can be performed in this way: starting with k vertices $z_{0,1}, z_{0,2}, \dots, z_{0,k}$ and a $(k - 1)$ -tuple of uniformly distributed and mutually independent random numbers $r_i \in [0, 1)$ for $i = 1, \dots, k - 1$, we perform the following sequence of assignments to calculate a point $z_{k-1,1} \in A$:

$$\begin{aligned} t_1 &= \sqrt[k-1]{r_1} \\ z_{1,1} &= (1 - t_1)z_{0,1} + t_1z_{0,2} \\ z_{1,2} &= (1 - t_1)z_{0,1} + t_1z_{0,3} \\ &\vdots \\ z_{1,k-1} &= (1 - t_1)z_{0,1} + t_1z_{0,k} \\ \hline t_2 &= \sqrt[k-2]{r_2} \\ z_{2,1} &= (1 - t_2)z_{1,1} + t_2z_{1,2} \\ z_{2,2} &= (1 - t_2)z_{1,1} + t_2z_{1,3} \\ &\vdots \\ z_{2,k-2} &= (1 - t_2)z_{1,1} + t_2z_{1,k-1} \\ \hline &\vdots \\ \hline t_{k-1} &= \sqrt[r_{k-1}]{} \\ z_{k-1,1} &= (1 - t_{k-1})z_{k-2,1} + t_{k-1}z_{k-2,2}, \end{aligned} \quad (9)$$

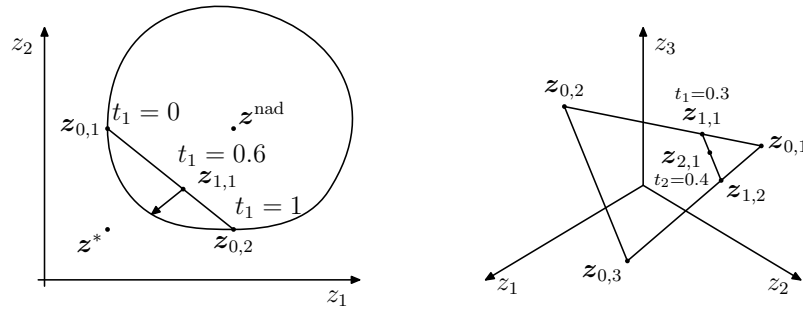


Fig. 6. Location of the reference set A in the two-dimensional and three-dimensional objective spaces.

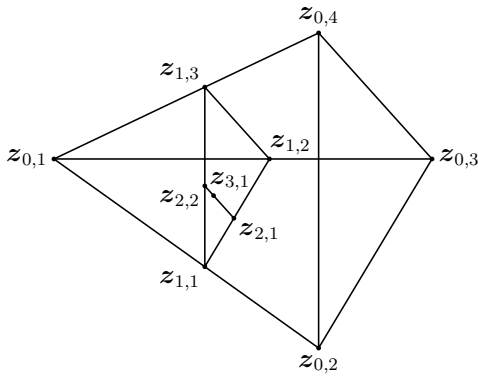


Fig. 7. Obtaining a point from the reference set for $k = 4$.

which can also be written in the more “algorithmic” notation

```

for  $i \leftarrow 1$  to  $k - 1$  do
  begin  $t_i \leftarrow \sqrt[k-i]{r_i}$ 
  for  $j \leftarrow 1$  to  $k - i$  do
     $z_{i,j} \leftarrow (1 - t_i)z_{i-1,1} + t_i z_{i-1,j+1}$ 
  end

```

(10)

This procedure therefore calculates a total of $N = \sum_{i=1}^{k-1} i = k(k-1)/2$ points $z_{i,j}$ in the k -dimensional objective space (i.e., $N = 1, 3$ and 6 points for $k = 2, 3$ and 4) from k initially known vertices of the reference set. An example of generation of a point ($z_{3,1}$) from a reference set in the shape of a tetrahedron (i.e., when $k = 4$) is shown in Fig. 7.

3. Application Examples

3.1 RF C-Class Power Amplifier Design

As a sophisticated example, let us try to design the last stage of an RF power amplifier for a narrow-band signal with an analog modulation at the frequency $f_1 = 300$ MHz. The source and load impedances should be both 50Ω and supply voltage $V_{DD} = 12$ V. Our goal will be to explore the trade-offs between achievable output power, power efficiency and total harmonic distortion.

3.1.1 Schematic

We use an RF N-channel LDMOS as an active component and a topology that is typical for C-class mode of operation, see Fig. 8. The transistor is followed by an LC filter to suppress harmonic distortion and provide good impedance matching. (Even though impedance matching at the output is not directly required, it is enforced indirectly by maximizing output power.) The combination of elements L_1 , C_1 and C_2 can also be seen as a tapped resonant circuit. As for the transistor, our choice will be LP821 (Polyfet RF Devices), a silicon LDMOS device for frequencies of up to 500 MHz, with a maximal total dissipated power of 50 W.

As our goal is exploration of the output trade-offs rather than obtaining a complete design, no input impedance matching circuit is considered, and no stability-ensuring measures are taken (other than rather small reactance of the capacitance between gate and source of the transistor itself).

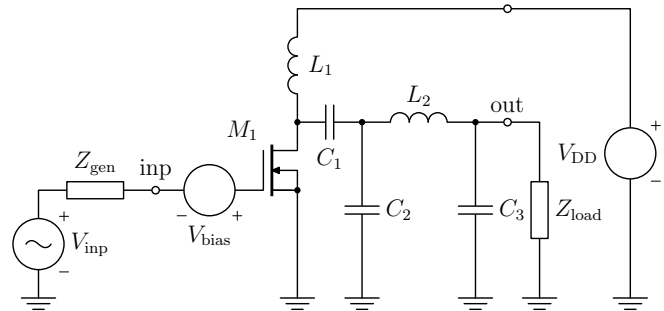


Fig. 8. C-class amplifier with optimized steady-state period.

3.1.2 Design Variables

As design variables we have two kinds of parameters: (A) parameters of the gate voltage that directly determine the operating mode of the transistor, and (B) all LC-component values of the filter.

A simple way to define the design variables of the former group would be the combination of the input AC voltage V_{inp} and its DC offset V_{bias} . That, however, would not provide direct control over the voltage between gate and source, which must not exceed 20 V (as given by maximum ratings of the device). This requirement would have to be

enforced by means of a special constraint, which would increase simulation time. In order to avoid this need, an estimated peak V_{gs} voltage, denoted by $V_{gs\max}$, was chosen as one design variable and the amplitude of its AC component as another one. The gate voltage estimate is defined using the equation of the voltage divider formed by the driver output resistance R_d and input capacitive reactance of the gate $X_i \approx 10 \Omega$

$$V_{gsACm} = V_{inpACm} \frac{X_i}{\sqrt{X_i^2 + R_d^2}} \quad (11)$$

where V_{inpACm} is the amplitude of the input AC voltage component from the preceding driver stage (open-circuited). From given values of design variables $V_{gs\max}$ and V_{gsACm} we then obtain

$$V_{bias} = V_{gs\max} - V_{gsACm}, \quad V_{inpACm} = V_{gsACm} \frac{\sqrt{X_i^2 + R_d^2}}{X_i} \quad (12)$$

Table 1 gives a summary of all design variables including their ranges and types of coverage.

No.	Symbol	Bound		Unit	Coverage Type
		Lower	Upper		
1	$V_{gs\max}$	2	20	V	lin.
2	V_{gsACm}	0.4	12	V	lin.
3	L_1	3 n	30 n	H	log.
4	C_1	10 p	300 p	F	log.
5	C_2	3 p	300 p	F	log.
6	L_2	3 n	100 n	H	log.
7	C_3	3 p	100 p	F	log.

Tab. 1. Design variables for the power amplifier.

3.1.3 Design Goals

There is a total of five design goals, three of which are the three objective functions to be optimized and two constraints representing maximum ratings of the LDMOS. All goals are defined in terms of waveforms of voltages and currents in the periodic steady state, which was obtained by the steady-state analysis of the simulator CIA [9] (necessary time-domain sensitivity analysis is also described in [10]). Table 2 gives a complete summary of all design goals. The individual design goal definitions are as follows:

No.	Symbol	Type	Direction	Optimum/ Bound	Unit
1	P_{out1}	obj.	max.	31.1	W
2	η	obj.	max.	83.0	%
3	THD	obj.	min.	0.0783	%
4	$I_{d\text{ avg}}$	constr.	\leq	5	A
5	P_{diss}	constr.	\leq	50	W

Tab. 2. Design goals for the power amplifier.

¹This is true also for so called Power-Added Efficiency (PAE), defined as the ratio $(P_{out} - P_{in})/P_{DC}$. PAE, however, has the disadvantage of not correctly describing the essence of amplification, which really consists in multiplying the signal power (at the expense of power supply) rather than adding to it. Consequently, it has a negative value when $P_{out} < P_{in}$, which can also be inconvenient in some cases.

a) Average output power at the first harmonic frequency P_{out1} .

$$P_{out1} = \frac{|\hat{v}_{out1}|^2}{2R_L} = \frac{a_1^2 + b_1^2}{2R_L} \quad (13)$$

where \hat{v}_{out1} is the phasor of the output voltage $v_{out}(t)$, a_k and b_k are generally the coefficients of the k -th cosine and sine harmonic (Fourier) components of the periodic steady-state output voltage $v_{out}(t)$ of the period T , respectively:

$$a_k = \frac{2}{T} \int_T v_{out}(t) \cos \frac{2\pi k}{T} t dt, \quad b_k = \frac{2}{T} \int_T v_{out}(t) \sin \frac{2\pi k}{T} t dt.$$

Here the integrals over period T were computed using the trapezoidal method of numeric integration.

b) Power efficiency η . It is defined as the ratio between the output power at the first harmonic frequency and the total average power from power supply and from the input driver. Such a form of definition encourages not only lower power dissipation on the transistor, but also lower input power and thus higher power gain¹:

$$\eta = \frac{P_{out1}}{\frac{V_{DD}}{T} \int i_{DD} dt + \frac{1}{T} \int v_{inp}(t) i_{inp}(t) dt} \times 100 \% \quad (14)$$

c) Total harmonic distortion THD .

$$THD = \sqrt{\frac{P_{out\text{ higher}}}{P_{out}}} \times 100 \% \quad (15)$$

where $P_{out\text{ higher}}$ is the output power at higher harmonics up to n_h

$$P_{out\text{ higher}} = \frac{1}{2R_L} \sum_{k=2}^{n_h} a_k^2 + b_k^2, \quad (16)$$

with $n_h = 10$, and where P_{out} is the total output power computed with the formula

$$P_{out} = \frac{1}{R_L} \left[\frac{1}{T} \int v_{out}^2(t) dt - \left(\frac{1}{T} \int v_{out}(t) dt \right)^2 \right] \quad (17)$$

The second term here cancels the contribution by a possible false DC component that could emerge as a result of the failure to fully achieve the periodic steady state within the chosen maximum number of iterations. (We know that in reality the DC component of the output voltage must be zero due to the capacitive coupling by C_1 and the load being linear.)

d) The maximum ratings of the transistor are applied as constraints. Maximum average drain current $I_{d\text{ avg}}$ and the maximum average dissipated power by the transistor P_{diss}

$$I_{d\text{ avg}} = \frac{1}{T} \int_T i_d(t) dt \quad (18)$$

and

$$P_{\text{diss}} = \frac{1}{T} \int_T [v_{gs}(t) i_g(t) + v_{ds}(t) i_d(t)] dt, \quad (19)$$

respectively, where $i_g(t)$, $i_d(t)$ are the instantaneous gate and drain currents, and $v_{gs}(t)$, $v_{ds}(t)$ are the instantaneous voltages between gate and source and drain and source.

3.1.4 Transistor Model

The model used for simulations is based on a SPICE-like one structured as shown in Fig. 9.

The original manufacturer's model is actually only the simple Level 1 SPICE MOSFET one (i.e., Shichman and Hodges). Therefore, its parameters were recalculated for using the semiempirical Level 3 model. They became $V_{TO} = 2.4$ V, $\phi_S = 0.6$ V, $\phi_O = 0.8$ V, $W = 0.04$ m, $L = 1$ μm , $X_J = 1$ μm , $X_{JL} = 0$ μm , $t_{\text{ox}} = 100$ nm, $N_{FS} = 0$ m⁻², $N_A = 10^{21}$ m⁻³, $v_{\text{max}} = 5 \times 10^4$ m/s, $\mu_O = 0.06$ m²/(Vs), $\varkappa = 0.22$, $E_P = 5 \times 10^5$ V/m, $K_P = 1.8 \times 10^{-5}$ A/V², $\gamma = 0$ $\sqrt{\text{V}}$, $\delta = \eta = \iota = 0$, $\theta = 0$ V⁻¹, $r_D = 0.16$ Ω , and $r_S = 0.16$ Ω – the manufacturer's value of W (for the composed devices like LDMOS, this number represents the element as a whole) clearly indicates that LP821 is really a power transistor. The manufacturer's values of the JFET and PN diode parameters were $\lambda = 0.8$ V⁻¹, $\beta = 6$ AV⁻², $V_{TO} = -5.25$ V, $C_{JOD} = C_{JOS} = 0$ F, $I_S = 10^{-14}$ A, $n = 1$, $V_B = 45$ V, $I_B = 10^{-7}$ A, $C_{JO} = 60$ pF, $\phi_O = 0.6$ V, and $m = 0.25$.

The RLC component values are the following: $L_{\text{GATE}} = 0.867$ nH, $R_{\text{GATE}} = 0.01$ Ω , $C_G = 3.5$ pF, $C_{\text{RSS}} = 4.5$ pF, $C_{\text{ISS}} = 22.1$ pF, $L_S = 0.108$ nH, $C_S = 0.43$ pF, $L_D = 0.51$ nH, $C_D = 0.01$ pF, $R_{\text{RC}} = 1989$ Ω , and $C_{\text{RC}} = 0.381$ nF.

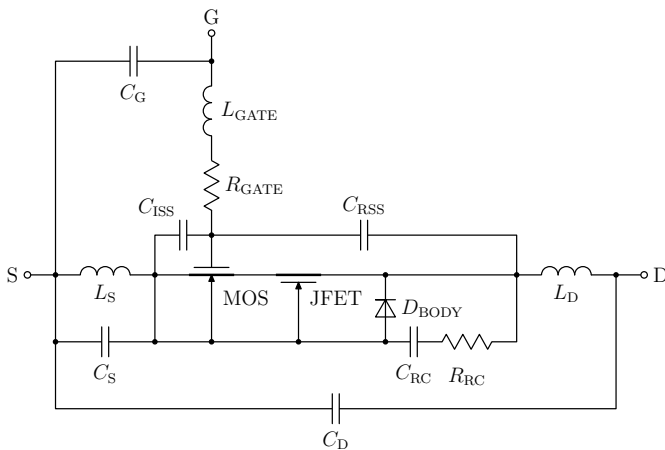


Fig. 9. Model configuration of LDMOS LP821.

3.1.5 Models of LC Components

Most design methods in network theory use idealized circuit elements, especially the passive ones. However, real-life elements have *always* parasitics attached to them that often substantially modify the circuit behavior at higher frequencies. Therefore, the parasitics should be somehow considered within used design procedures. One approach would be to first assume ideal elements without the parasitics, and after determining their values (e.g., by using optimization) and adding the parasitics afterwards to apply a correction to each component value so that its impedance at a chosen frequency is close to that of the ideal element in the design.

A more thorough and correct approach, however, is to introduce the parasitics already before the optimization by using parametrized RF models instead of simple ideal elements. Such a procedure is called *parasitic-aware optimization* [11]. It was chosen to be applied to all LC components in the present example. Fig. 10 shows used model structures for inductors and capacitors.

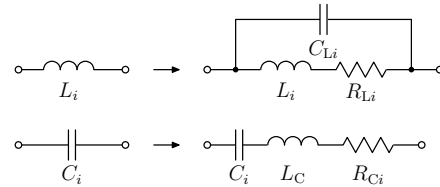


Fig. 10. Modeled parasitics of passive components.

Only rough estimates of parasitics and their dependences on the main component values have been introduced, as real parameters and functions strongly depend on types and spatial configuration of the real components, their lead lengths, etc. Each inductor L_i , $i = 1$ and 2 has a series resistance R_{Li} representing all kinds of power losses (due to skin effect, eddy currents and/or coil core hysteresis, etc.) and a parallel capacitance C_{Li} modeling the collective stray capacitance (between the coil's winding turns, leads, etc.), whose values are obtained using formulas

$$R_{Li} = \frac{2\pi f_1 L_i}{Q_{L\text{max}}} + R_{L0} \quad \text{and} \quad C_{Li} = L_i p_{CL} + C_{L0}. \quad (20)$$

Here the frequency $f_1 = 300$ MHz; the maximum quality factor $Q_{L\text{max}} = 100$, achievable only when the constant term $R_{L0} = 10$ m Ω is negligible; the stray capacitance coefficient $p_{CL} = 1$ pF/ μH and the constant term $C_{L0} = 100$ fF.

Similarly, each capacitor C_i , $i = 1, 2$, and 3 has a series resistance R_{Ci} (also known as ESR)

$$R_{Ci} = \frac{1}{2\pi f_1 C_i Q_{C\text{max}}} + R_{C0} \quad (21)$$

where $Q_{C\text{max}} = 1000$ and $R_{C0} = 10$ m Ω ; and a stray series inductance L_C (ESL) estimated by a constant value of 3 nH.

Even though those formulas and parameter values are very approximate, they still represent a significant improvement to the whole method, at least, by helping to keep the component values in the design after optimization in realistic proportions. For example, inductances will not tend to

be too large, as their own resonant frequencies need to stay above the basic signal frequency f_1 (and probably also above some higher harmonic frequencies).

3.1.6 Results

Fig. 11 shows a total of 84 obtained solutions covering the three-dimensional Pareto front. There is obviously a large trade-off between harmonic distortion and power efficiency at the highest output power levels, but it diminishes with decreasing the output power, and for $P_{out1} \leq 14\text{ W}$ the requirement of low distortion can be met with almost no penalty on power efficiency.

Instead of by type of points, the different THD bounds can be distinguished by separating the particular cases into an array of graphs. Such an alternative format is presented in Fig. 13.

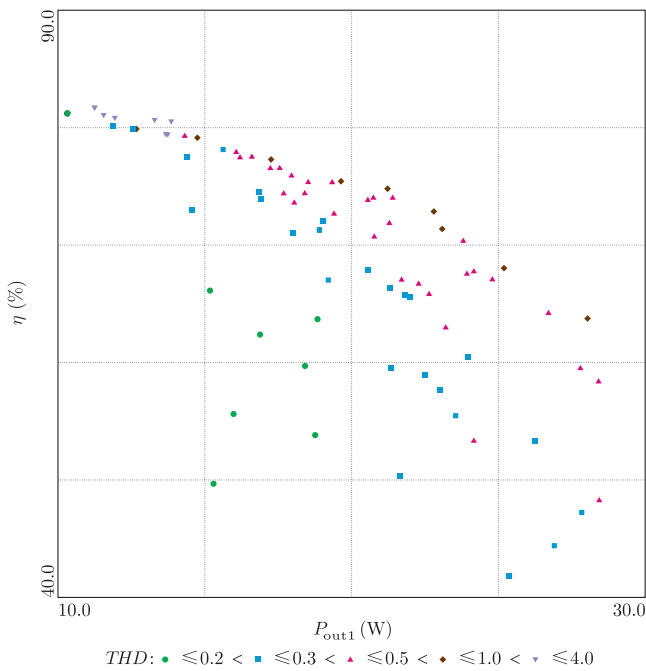


Fig. 11. Obtained Pareto front in the space P_{out1} , η , THD .

A selection of five distinctly different solutions is given in Tab. 6: number 1 has the lowest distortion THD , 4 has one of the highest values of P_{out1} , and 5 the highest efficiency η ; solutions 2 and 3 are located in the middle area at different levels of THD .

Instead of trying to uniformly cover the three-dimensional Pareto front, it may be preferable to cover only a set of its two-dimensional contours. This can be done by having THD as a constraint (instead of as objective function) and by repeating the optimizations for different THD bound values. Alternately, if we already have a set of solutions such as of Fig. 11, we can obtain the solution covering the contours by reoptimizing them to the new set of constraints that includes THD , i.e., by running a new optimization with each already available solution as a starting point. A result of such a procedure is shown in Fig. 12.

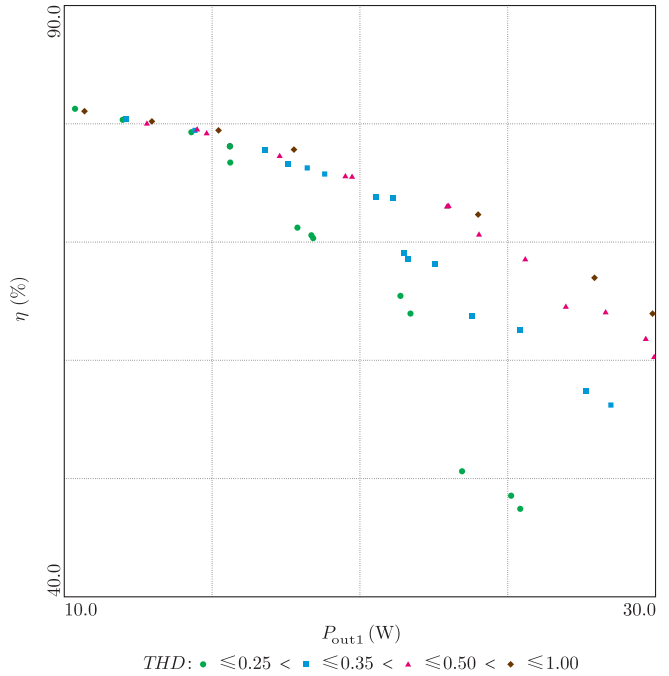


Fig. 12. The 3D Pareto front obtained in the form of contours.

No.	Symbol	Solution Number					Unit
		1	2	3	4	5	
1	V_{gsmax}	9.97	15.9	20.0	19.2	18.9	V
2	V_{gsACm}	4.03	8.05	10.7	9.24	12.0	V
3	L_1	7.86 n	11.3 n	4.23 n	3.97 n	5.03 n	H
4	C_1	294 p	133 p	299 p	51.6 p	166 p	F
5	C_2	22.6 p	5.09 p	27.0 p	300 p	3.41 p	F
6	L_2	6.84 n	7.00 n	7.97 n	7.32 n	9.89 n	H
7	C_3	20.1 p	2.35 p	18.4 p	22.6 p	17.0 p	F
1	P_{out1}	15.3	18.8	22.8	28.4	11.2	W
2	η	49.7	63.7	72.9	58.4	81.7	%
3	THD	0.163	0.239	0.512	0.394	3.03	%
4	$I_{d\ avg}$	2.56	2.44	2.59	4.01	1.15	A
5	P_{diss}	13.6	8.42	6.65	16.0	1.84	W

Tab. 3. Selected five solutions from the various parts of the Pareto front with respective values of the design goals.

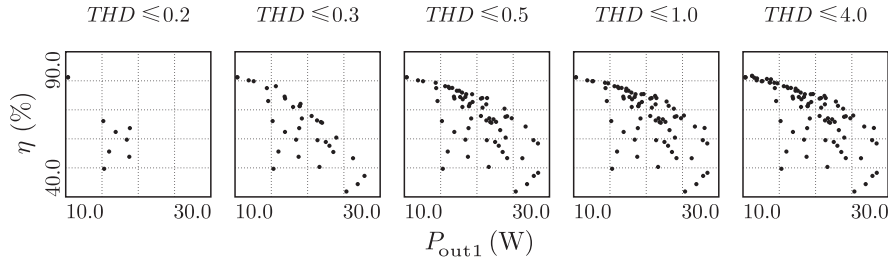


Fig. 13. An alternative way of displaying the three-dimensional Pareto front by the sequence of plots for various THD.

3.2 Four-Dimensional Task – Video Amplifier

We are to optimize a video amplifier [12] in Fig. 14 with an input matched to a source impedance 75Ω , with its output able to drive a 75Ω load, and with $1 V_{pp}$ output capability. The 3 dB roll-off frequency f_m should be as high as possible, the low-frequency voltage gain A_v should be positive and of the biggest possible value, and the total DC supply current I_{cc} should be as low as possible. As the decision variables, we will use the resistances R_1 – R_5 (only a range of positive values is allowed). We assume that the capacitors C_1 – C_3 have sufficiently large capacitances not to influence the low frequency gain. All high-frequency gain characteristics are thus determined only by inner capacitances of the transistors. The type 2N5179 was prescribed for both Q_1 and Q_2 , and the Gummel-Poon model was used.

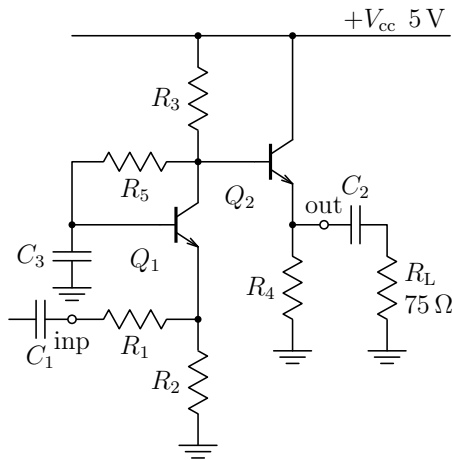


Fig. 14. Video amplifier schematic.

As a measure of the impedance matching, a low-frequency voltage standing wave ratio SWR was used:

$$SWR = \frac{1 + |\rho|}{1 - |\rho|}, \quad \rho = \frac{R_i - 75 \Omega}{R_i + 75 \Omega}. \quad (22)$$

The multiobjective optimization task is then following:

$$\begin{aligned} &\text{minimize} && SWR, I_{cc} \\ &\text{maximize} && A_v, f_m \\ &\text{subject to} && V_{out} \leq 3.5 V \end{aligned} \quad (23)$$

where the constraint condition concerning the output voltage V_{out} ensures the required $1 V_{pp}$ output capability.

Before we start the proper multi-objective optimization, it is a good idea to examine the best values z_i^o attainable by the four optimized characteristics if they are optimized alone. We *a priori* know that $SWR^o = 1$, because with a suitable value of R_1 , the input resistance R_i can be made exactly equal to 75Ω . It is also clear that $I_{cc}^o \rightarrow 0$ mA. For A_v , the independent maximum value was found to be $A_v^o = 40.72$ dB, for which $R_i = 18.41 \Omega$, $SWR = 4.073$, $I_{cc} = 1.346$ mA and $f_m = 350.7$ MHz; and the maximum f_m is found $f_m^o = 860.3$ MHz, for which $R_i = 546.1 \Omega$, $SWR = 7.282$, $A_v = 4.281$ dB, and $I_{cc} = 7.532$ mA.

3.2.1 Usage of the Goal Attainment Method

The following choice of the four objective functions was naturally created first:

$$\begin{aligned} f_1 &= 10(SWR - 1), & f_3 &= \frac{I_{cc}}{1 \text{ mA}}, \\ f_2 &= A_v^o - A_v, & f_4 &= \log \frac{f_m^o}{f_m}. \end{aligned} \quad (24)$$

A simple penalty function method is used to convert the constrained optimization problem into an unconstrained one. In this method, constraints are enforced by means of additive components called penalty functions, increasing the resulting objective function, and which are progressively dependent on the amount of the violation of the constraints. Only one constraint applies in our case, and is expressed by a penalty function

$$c_1 = \max \left(\frac{V_{out} - 3.5 V}{3.5 V}, 0 \right) \times q \quad (25)$$

where q is a coefficient controlling how much the constraint component is emphasized over the usual minimized components in the objective function.

The functions f_1 through f_4 defined above can be directly used in some other multi-objective methods, e.g., in NSGA-II [7] or Weighted Sum Method (WSM) [8]. However, for a usage of the Goal Attainment Method, we created four new penalty functions related to the functions f_i where $q = 100$ is used in a standard way:

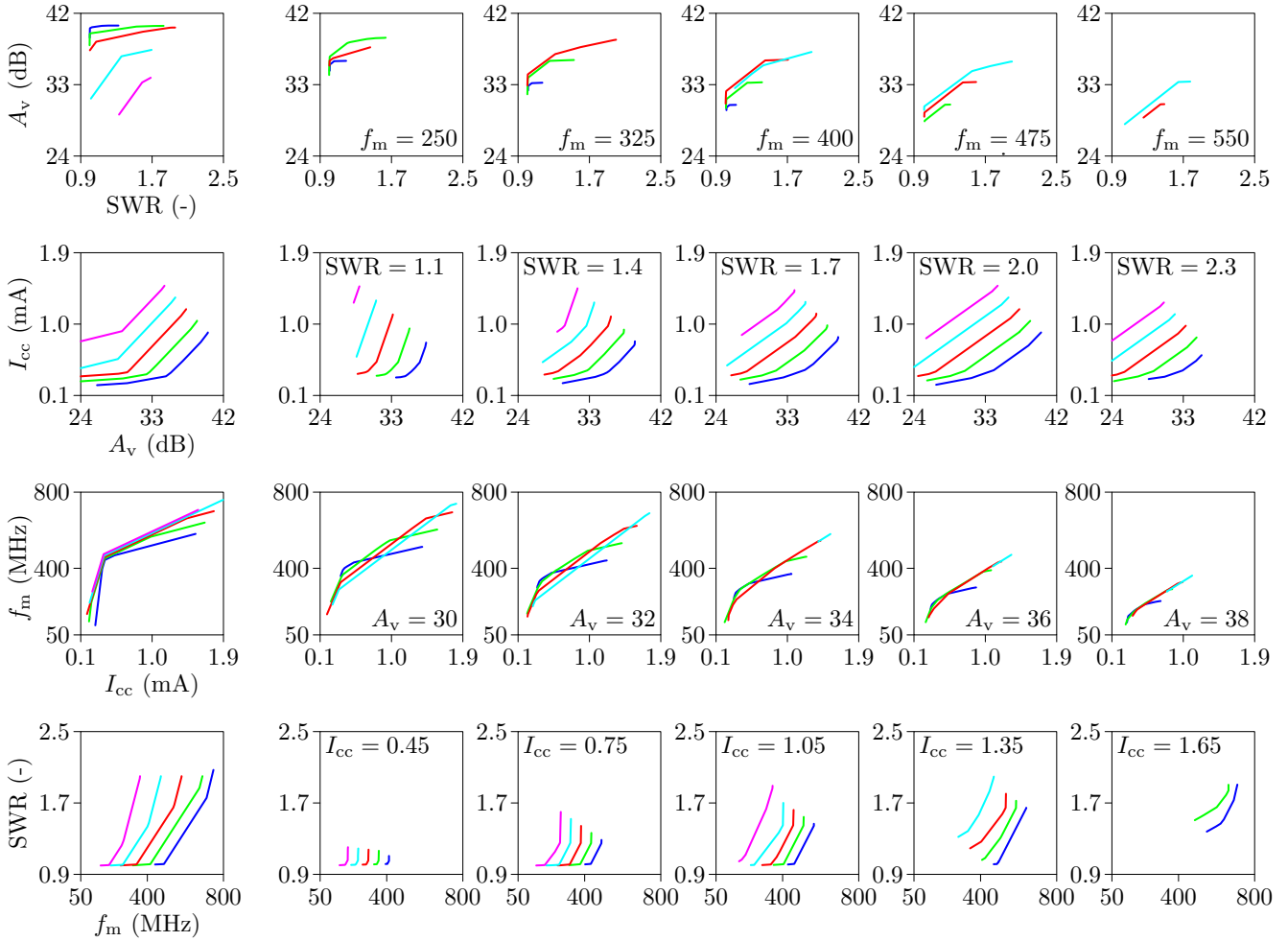


Fig. 15. A quasi 4-dimensional graph of Pareto front. One objective was chosen as a graph parameter (f_m , SWR, A_v , and I_{cc} in the first, second, third, and fourth rows, respectively), and five equidistant sampling levels of it were chosen to cover a significant part of its range. The curves in the first row represent non-inferior points for the currents I_{cc} 0.45, 0.75, 1.05, 1.35, and 1.65 mA, respectively. The curves in the second row represent non-inferior points for the frequencies f_m 250, 325, 400, 475, and 550 MHz, respectively. The curves in the third row represent non-inferior points for the standing wave ratios SWR 1.1, 1.4, 1.7, 2.0, and 2.3, respectively. The curves in the fourth row represent non-inferior points for the amplifications A_v 30, 32, 34, 36, and 38 dB, respectively. The first part (aggregate graph) represents the case when the values of one dimension are ignored, which is another way to decrease the plot dimensionality; see the explanation below.

$$\begin{aligned}
 g_1 &= \max \left(\frac{10(\text{SWR} - 1) - w_1\gamma - P}{P}, 0 \right) \times q, \\
 g_2 &= \max \left(\frac{A_v^o - A_v - w_2\gamma - P}{P}, 0 \right) \times q, \\
 g_3 &= \max \left(\frac{I_{cc}/1 \text{ mA} - w_3\gamma - P}{P}, 0 \right) \times q, \\
 g_4 &= \max \left(\frac{\log(f_m^o/f_m) - w_4\gamma - P}{P}, 0 \right) \times q
 \end{aligned} \tag{26}$$

with the single objective function to be minimized, i.e., $f(\mathbf{x}) = \gamma$. The constraint penalty function c_1 (25) remains in action.

Note that, for simplicity, we have set all the design goals z_i^* equal to the same scalar value P . This is allowed by the special choice of the objective functions f_i in their definition. The single minimized objective function is then

formed as follows:

$$f_P^{\text{GAM}}(\mathbf{x}) = \gamma^2 + \sum_{i=1}^4 g_i^2(\mathbf{x}) + c_1^2(\mathbf{x}). \tag{27}$$

The objective function f_P is minimized using our original modification of the Levenberg-Marquardt method [13], which consists in normalizing the Jacobian matrix for suppressing numerical instability. The Levenberg-Marquardt method is used to obtain solutions for chosen values of w_i and P in (26). The iterations typically end when the maximum relative change in the decision variables between iterations is less than 10^{-4} or after reaching a maximum allowed number of iterations. For circuit simulations, our original software tool was used for the analysis with large efficiency enhancement by fill-in suppression.

3.2.2 Graphical Presentation of Results

As the objective region is a certain subset of a four-

dimensional space, its direct graphical presentation in two dimensions is impossible. However, the indirect way of plotting is possible, and it can be a useful tool in the stage of assessment of the available trade-offs. Fig. 15 shows independent rows of plots, each representing a different set of choices of individual objectives being placed at different axes or used as parameters.

The plots were obtained under the assumption of convex Pareto front and the exact procedure used is as follows. A total of 78 obtained solution points was gathered. Ten detected inferior points were removed thus leaving 68 points for further processing. One objective was chosen as a plot parameter (e.g., f_m in the first row) and five equidistant sampling levels of it were chosen to cover a significant part of its range. For each of the five sampling levels, the 68 points were then divided into two groups based on whether they are located below or above the sampling level. Then for all pairs of points such that the first point belongs to the first group and the second point belongs to the second group, interpolation points corresponding to the sampling levels were determined. As all the interpolation points have one coordinate of the same value, they can be considered to belong to the same three-dimensional space. We are not interested in the whole 3D body but only in the part of its surface representing the Pareto front. Therefore, the inferior points of this new set were also removed. In this way we have reduced the four-dimensional problem to three dimensions and the next step is to apply the same procedure further to obtain sets of two-dimensional curves.

Another way of creating plots of smaller dimensionality is simply to ignore the values of one dimension. (This is also done by the same program.) In this case, we do not produce the three-dimensional bodies by interpolation, but simply by using the original set of points. These *aggregate graphs* were added in Fig. 15 at the beginning of each row with the same configuration of axes, separated by a wider gap.

3.2.3 Comparing With Weighting Method

We have also compared the properties of our modification of the GAM procedure with the simpler WSM one [8]. In this case, the four objective functions (24) remain in action as well as the penalty function (25). However, the resulting single objective function is simpler

$$f_P^{\text{WSM}}(\mathbf{x}) = \sum_{i=1}^4 w_i f_i^2(\mathbf{x}) + c_1^2(\mathbf{x}), \quad (28)$$

and with the usual normalizing condition $\sum_{i=1}^4 w_i = 1$.

We have found that the objective values can be well controlled by the choice of w_i . However, even in the best case observed, about 20 % of changes in w_i have the opposite effect on the related goal than expected. Also, in few cases, the obtained solutions were found to be inferior to the ones with a different weighting vector.

3.3 Low-Noise Antenna Amplifier Design in the Frequency Domain

Let us consider a design of a low-noise antenna preamplifier for the frequency range of 50 MHz to 500 MHz. The nominal antenna as well as load impedances are 75Ω , supply voltage $V_{\text{supp}} = 12 \text{ V}$. We will assume that linearity is not a concern as the levels of received signals will be small. Our requirements on the design are to maximize the amplifier power gain while minimizing its noise figure. It will be a two-dimensional task with four constraints.

3.3.1 Schematic

For simplicity, we choose a single stage topology, using the bipolar transistor BFR90A in the common emitter configuration shown in Fig. 16. In this schematic, in fact, various elements of several similar designs found in the literature are combined:

- input impedance matching network,
- emitter degeneration network,
- DC biasing network, possibly introducing frequency-dependent feedback,
- output impedance matching network and linearity matching.

Even though some of these provisions (impedance matching, linearity) are not directly part of the initial set of requirements (min. noise, max. gain), all components present can have an impact on them (positive or negative). Therefore the strategy applied here is to let the optimization process choose which components are really necessary, despite the fact that some of them could have been dropped already at the beginning.

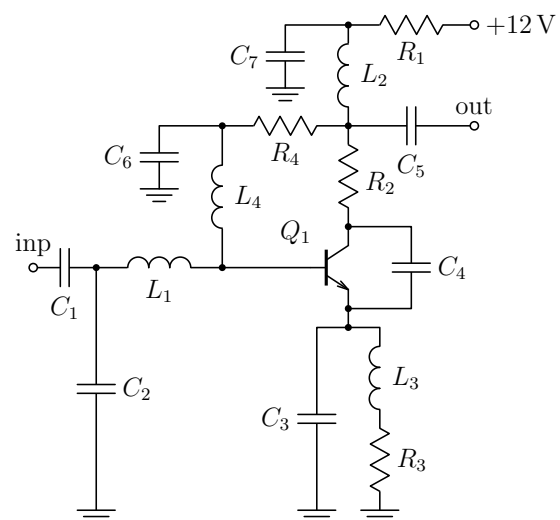


Fig. 16. Low-noise amplifier schematic.

3.3.2 Design Variables

The values of all passive components are to be determined by the optimization, therefore we have a design variable for each of them, as shown in Table 4. They are mostly restricted to ranges of two decades, covered logarithmically.

No.	Symbol	Bound		Unit	Coverage Type
		Lower	Upper		
1	C_1	10 p	10 n	F	log.
2	C_2	1 f	10 p	F	log.
3	L_1	1 n	100 n	H	log.
4	C_3	1 f	10 n	F	log.
5	L_3	100 p	100 n	H	log.
6	R_3	1 m	100*	Ω	log.
7	C_4	100 f	10 p	F	log.
8	R_2	1 m	100	Ω	log.
9	L_2	1 p	1 μ	H	log.
10	C_7	1 f	100 n	F	log.
11	R_1	10	1 k	Ω	log.
12	R_4	10 k	1 M	Ω	log.
13	C_6	1 f	1 n	F	log.
14	L_4	1 f	1 μ	H	log.
15	C_5	10 p	10 n	F	log.

* (R_3 was later fixed at its lower bound 1 m Ω)

Tab. 4. Design variables for the low-noise amplifier.

3.3.3 Design Goals

The set of design goals used for optimization consists of the two explicit requirements given in the assignment used as objective functions and some additional constraints to help to ensure a feasible design. See Table 5 for a complete summary of all design goals.

All frequency-dependent results are determined as the worst-case values over the full frequency range 50 MHz to 500 MHz. Most of those objective functions were evaluated using the amplifier s-parameters with the characteristic impedance $Z_c = 75 \Omega = R_{S1} = R_{S2} = R_{L1} = R_{L2} = R_{NS}$, obtained by AC analysis applied to the network shown in Figure 17. Two instances of the amplifier sub-circuit were analyzed simultaneously so that all four s-parameters could be determined in a single simulator run.

No.	Symbol	Type	Direction	Optimum/ Bound	Unit
1	A_{pt}	obj.	max.	17.5	dB
2	NF	obj.	min.	1.10	dB
3	I_c	constr.	\leq	20	mA
4	P_{diss}	constr.	\leq	150	mW
5	k_{Rs}	constr.	\geq	1.1	—
6	Δ	constr.	\leq	0.9	—

Tab. 5. Design goals for the low-noise amplifier.

a) Transistor Maximum Ratings For the amplifier to stay operable, all maximum ratings of the transistor must be met. Therefore the following constraints on the collector current I_c and total dissipated power P_{diss} have been introduced into the optimization: $I_c \leq 20$ mA, and $P_{diss} \leq 150$ mW.

b) Transducer Power Gain A_{pt} , defined as the ratio, expressed in dB, of the actual power entering the load and the available power of the source of the input signal. It was computed using the formula

$$A_{pt} = 20 \log \frac{2|\hat{v}_{21}|}{|\hat{v}_{S0}|} = 20 \log |\hat{s}_{21}| \quad (29)$$

where $|\hat{v}_{21}|$ is the amplitude of the output voltage and $|\hat{v}_{S0}|$ is the amplitude of the input signal source (open circuited). (If the amplitude $|\hat{v}_{S0}|$ is chosen equal to 2, the value of $|\hat{v}_{21}|$ is directly equal to the gain.)

c) Noise Figure NF , defined as the ratio (in dB) of the total spectral noise power density available at the amplifier output and of its part obtained by (noiseless) amplification of the input power spectral density, assumed to be thermal noise at a reference temperature T_0 . This definition was fulfilled by the formula

$$NF = 20 \log \frac{v_{Nout} |\hat{v}_{S0}|}{v_{NS0} |2\hat{v}_{21}|} \quad (30)$$

where \hat{v}_{S0} and \hat{v}_{21} have the same meaning as in the previous formula, v_{Nout} is the narrow-band noise voltage in V/\sqrt{Hz} on the load (where the load itself is noise-free) and v_{NS0} is the noise voltage measured on an separate unloaded noisy resistor at $T_0 = 300$ K of the same resistance as has the input signal source, i.e., 75 Ω .

d) Stability Another necessary condition for the amplifier to be useful is the requirement of stability. One way of dealing with this issue typically used in RF circuits is ensuring that the amplifier is *absolutely stable*, i.e., stable not only for the typical source and load impedances but also for any combination of (passive) impedances terminating both ports. Absolute stability can be easily tested using Rollet Stability Factor k_{Rs} :

$$k_{Rs} = \frac{1 + |\Delta|^2 - |\hat{s}_{11}|^2 - |\hat{s}_{22}|^2}{2|\hat{s}_{12}\hat{s}_{21}|} > 1$$

and

$$\Delta = \det \mathbf{s} = |\hat{s}_{11}\hat{s}_{22} - \hat{s}_{12}\hat{s}_{21}| < 1.$$

For practical design, these theoretical thresholds were provided with 10 % margins, yielding 1.1 and 0.9, as shown in Tab. 5.

All four s-parameters are computed from the voltage phasors of Fig. 17 using the formula

$$\mathbf{s} = \begin{pmatrix} \hat{s}_{11} & \hat{s}_{12} \\ \hat{s}_{21} & \hat{s}_{22} \end{pmatrix} = \begin{pmatrix} \frac{2\hat{v}_{11}}{\hat{v}_{S0}} - 1 & \frac{2\hat{v}_{12}}{\hat{v}_{S0}} \\ \frac{2\hat{v}_{21}}{\hat{v}_{S0}} & \frac{2\hat{v}_{22}}{\hat{v}_{S0}} - 1 \end{pmatrix}$$

which simplifies to

$$\begin{pmatrix} \hat{v}_{11} - 1 & \hat{v}_{12} \\ \hat{v}_{21} & \hat{v}_{22} - 1 \end{pmatrix}$$

if we choose $\hat{v}_{S0} = 2$.

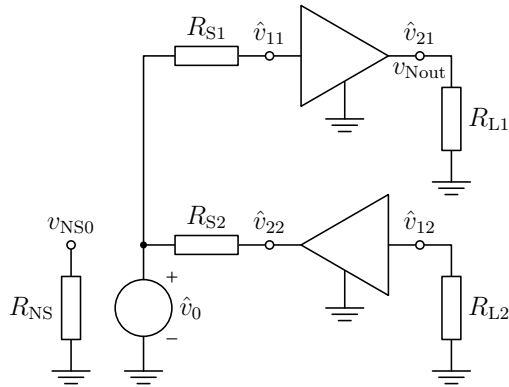


Fig. 17. Auxiliary network used for computing S parameters and noise figure.

3.3.4 Results

A total of 187 solutions has been obtained, uniformly covering the Pareto front as shown in Fig. 18. In this graph, we can distinguish three typical areas:

1. low gain area, $A_{pt} < \text{approx. } 17 \text{ dB}$, where noise figure is good, but gain A_{pt} is too small,
2. middle area, where with increasing gain the noise figure starts to increase significantly, and
3. high noise figure area, $NF > 2 \text{ dB}$, where the noise figure increases with such a rate that in no longer justifies the corresponding increases in gain.

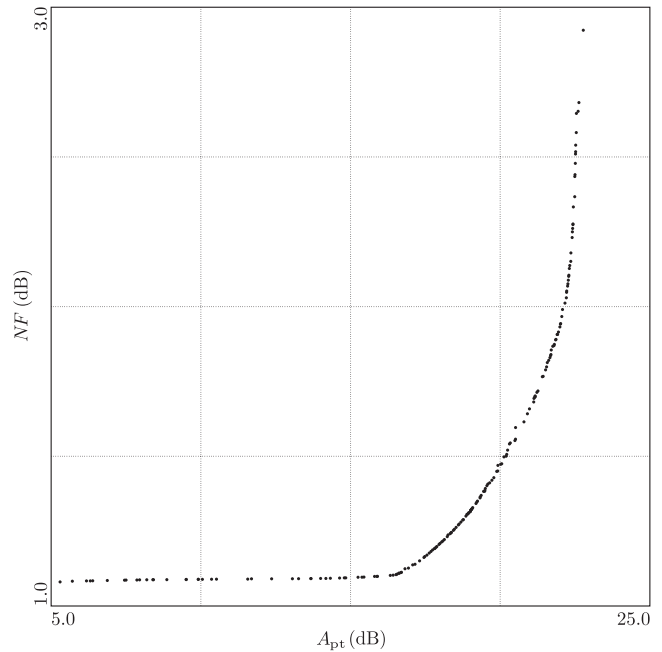


Fig. 18. Obtained Pareto front in the objective space A_{pt} and NF .

Obviously a reasonable tradeoff between the two objectives can only be found in the middle area.

Table 6 presents a selection of five solutions ordered by ascending transducer gain A_{pt} , spanning over all of the three areas. Solutions 2, 3 or 4 would be good candidates for a final choice of a single solution, depending on the designer's (or the decision maker's) preferences.

No.	Symbol	Solution Number					Unit
		1	2	3	4	5	
1	C_1	10.0 n	10.0 n	10.0 n	7.78 n	182 p	F
2	C_2	20.3 f	1.00 f	2.90 p	3.17 p	5.37 p	F
3	L_1	21.3 n	14.9 n	22.5 n	18.5 n	19.2 n	H
4	C_3	2.45 f	1.71 f	4.70 p	37.0 f	1.00 f	F
5	L_3	3.57 n	1.07 n	615 p	422 p	295 p	H
6	R_3	1.00 m	1.00 m	1.00 m	1.00 m	1.00 m	Ω
7	C_4	2.07 p	2.55 p	2.42 p	2.53 p	1.09 p	F
8	R_2	9.51 m	1.00 m	14.7 m	3.16 m	7.62 m	Ω
9	L_2	168 n	51.2 n	40.1 n	36.9 n	60.6 n	H
10	C_7	3.20 p	5.33 p	5.85 p	6.88 p	2.50 p	F
11	R_1	293	80.3	50.9	43.9	136	Ω
12	R_4	331 k	260 k	145 k	87.6 k	55.1 k	Ω
13	C_6	1.34 p	404 f	987 f	1.35 f	76.9 f	F
14	L_4	1.00 f	1.00 f	1.00 f	1.00 f	1.00 μ	H
15	C_5	100 p	3.98 n	4.91 n	5.01 n	10.0 n	F
1	A_{pt}	14.8	18.0	20.0	21.5	22.5	dB
2	NF	1.09	1.21	1.47	1.80	2.36	dB
3	I_c	2.96	4.00	7.09	11.5	15.1	mA
4	P_{diss}	32.9	46.7	82.5	132	150	mW
5	k_{RS}	1.06	1.10	1.10	1.10	1.09	—
6	Δ	0.467	0.302	0.335	0.351	0.404	—

Tab. 6. Five selected solutions from the Pareto front with the results shown in Fig. 19.

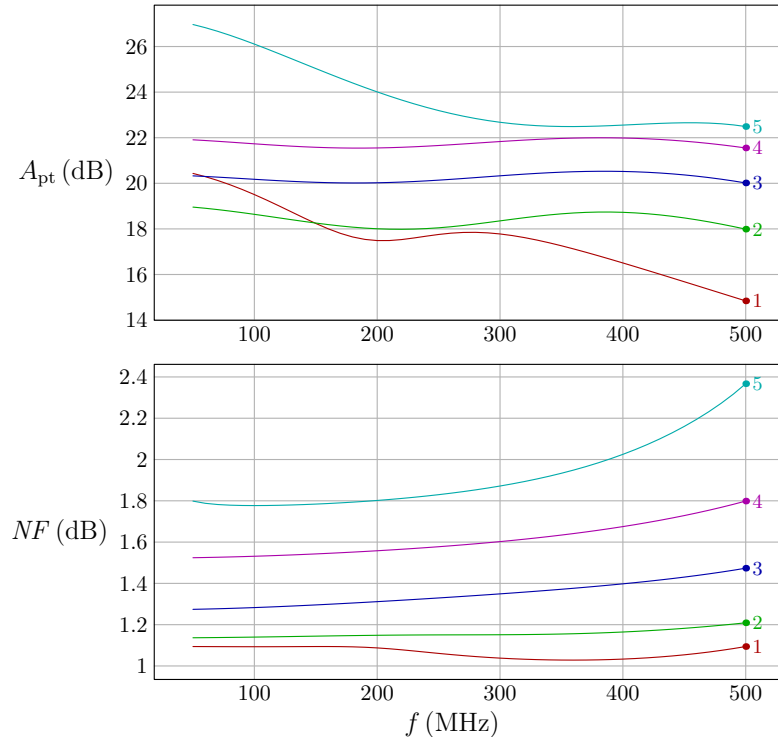


Fig. 19. Low-noise amplifier A_{pt} and NF plots for the five selected solutions from Tab. 6.

From the results in the table we can see that, as expected, some components have (almost) zero values and thus can be omitted from the schematic. This is especially true for resistors R_2 and R_3 , corresponding with the fact that no linearity requirements were present in the used set of design goals. We can also see that not all constraints became active: only P_{diss} and k_{Rs} did, the former only for solution No. 5.

Figure 19 presents the frequency plots for both of the objective functions and for all five selected solutions. From the plots it is obvious that the higher end of the frequency range tends to be the most critical for both gain and noise figure.

We may conclude stating that the applied multiobjective optimization method succeeded in finding both the location as well as shape of the Pareto front even for such a relatively high number of design variables and wide ranges of their values.

4. Using Metaheuristics in Mono- and Multiobjective Methods

4.1 Characterization of the Metaheuristics

This new kind of methods – which are sometimes based on ideas of everyday life – has been developed to solve difficult optimization problems. These methods include genetic algorithms (GA), simulated annealing (SA), ant colony al-

gorithms, or particle swarm optimization (PSO). They have been created to overcome frequent serious problems of “classical” iteration algorithms. For example, an escape from a local minimum is possible in “distributed” metaheuristics such as genetic algorithms [3]. On the other hand, the efficiency of these methods is often unpredictable. Therefore, the current tendency is towards the use of hybrid methods.

The use of metaheuristic methods for the analog circuit design has been described in a comprehensive way in [14, 15] – [14] considers merging GA/SA, [15] exploits non-sorting genetic algorithm (NSGA-II) and multiobjective evolutionary algorithm based on decomposition (MOEA/D). Some state-of-the-art hybrid methods are defined in [4] and [16].

In [17], a novel Pareto frontier covering strategy for the functional-specialization multiobjective genetic algorithm (FS-MOGA) has been presented, and the FS-MOGA method has been compared with the conventional NSGA-II one. In [18], a novel two-step searching method based on particle swarm optimization has been suggested for many-objective optimization problems, and the proposed algorithm has been compared with the NSGA-II, Sigma (PSO), and Sierra (PSO) ones. Moreover, a new hybrid method between differential evolution and genetic algorithm has been suggested in [19], i.e., coupling the genetic algorithm (GA), differential evolution (DE), and particle swarm optimization (PSO), and a comprehensive comparison of the hybrid algorithms (GA/PSO, DE/PSO, GA/DE, and GA/DE/PSO) with the pure ones (pure GA, DE, and PSO) has been performed. Another efficient way for the circuit synthesis consists in coupling the design rules with single optimization steps [20].

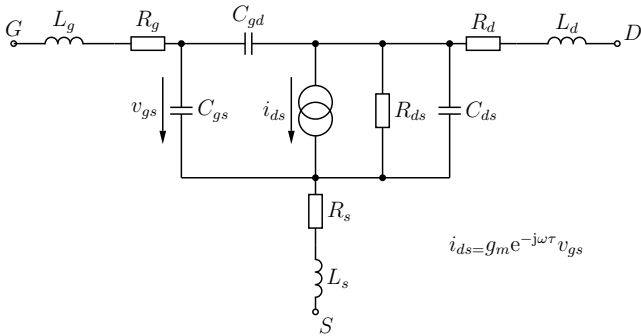


Fig. 20. Equivalent twelve-parameter linear circuit of pHEMT.

4.2 Comparing Metaheuristic Methods with the Classical Ones

For solving the examples in subsections 3.1, 3.2, and 3.3, the “classical” optimization methods were reliable and effective. The only problem has emerged with the numerical stability of the algorithm for solving systems of nonlinear differential-algebraic equations of the C-class amplifier in Fig. 8. Although the maximal order of polynomial interpolation could theoretically be six, we had to decrease it for some points of the Pareto front in Fig. 13 to a lower value, even to *one* in some critical cases. (The *A*-stability of the algorithms for the numerical integration is still under research [21].)

However, for certain more complex tasks, the metaheuristic methods must be used at least with a combination with the classical ones. Such a problem has been a determination of both static and dynamic model parameters of a 110-GHz pHEMT using measured multi-bias *s*-parameters [22]. Solving this problem, four methods have been compared: Levenberg-Marquardt (LM), genetic algorithm (GA), simulated annealing (SA), and Nelder-Mead (NM) simplex ones.

For a statistical comparison of these four optimization methods, twelve parameters of the model in Fig. 20 have been looked for. The goal functions are defined as multi-sum of differences between measured and identified *s*-parameters

$$\text{rms}_\ell = \sqrt{\frac{1}{4m} \sum_{k=1}^m \sum_{j=1}^2 \sum_{i=1}^2 \left(\frac{s_{ij,\ell}^{\text{meas}}(\omega_k) - s_{ij,\ell}^{\text{ident}}(\omega_k)}{|s_{ij,\ell}^{\text{meas}}(\omega_k)| + \text{null}_s} \right)^2} \quad (31)$$

where $\ell = 1, \dots, n$ denotes operating points for which the *s*-parameters have been measured (for identifying a *nonlinear* model [22], multi-operating-point data is always necessary, and $n \gg 1$), m is a number of frequencies at which they have been measured, and a tiny value null_s was set to 10^{-6} .

Let us now suppose that we know a vector \mathbf{x}^* for which (31) is minimal, and the lower and upper boundary vectors \mathbf{x}^L and \mathbf{x}^H of permitted parameter space are assigned with a variable factor as $\mathbf{x}^H = \mathbf{x}^* \times \text{factor}$, $\mathbf{x}^L = \mathbf{x}^* / \text{factor}$, respectively. The factor has been sequentially set to 1.2, 1.5, 2, 5, 10, 20, 50, 100, 200, and 500, and for each of these values, thirty optimizations have been performed with a starting point \mathbf{x}^0 chosen randomly (uniform distribution in

the allowed interval has been used). In this way, thirty various root-mean-square values have been obtained by (31), and minimal, mean, and standard deviations for them have been determined with the results shown in Figs. 21–23.

Fig. 21 (minimal deviations) shows that only SA has achieved $\text{rms}_{\text{min}} < 0.1$ for all the factor values, whereas LM has achieved the same results with the exception of the last value of factor. The other two methods have been considerably worse. Furthermore, Fig. 22 (mean deviations) shows that for the locally convergent methods LM and NM, rms_{mean} has grown in the similar way. On the contrary, for SA, $\text{rms}_{\text{mean}} > 0.1$ only for factor ≥ 200 . Finally, Fig. 23 (standard deviations) shows that the globally convergent methods have had very small dispersion at the end of the task, which means low dependence on the choice of \mathbf{x}^0 .

For this particular circuit, SA is the most robust method reaching the minimum regularly even with higher factor. On the other hand, LM is very efficient method when the starting vector is sufficiently near the optimum. Therefore, we have finally suggested a three-step hybrid method SA/LM that is described in a detailed way in [22] together with the results.

5. Conclusions

A novel reliable semiautomatic algorithm has been created and successfully implemented for the multiobjective optimization in both time and frequency domains. The procedure is based on an asymptotically uniform coverage of the reference set in a combination with modified goal attainment method with intention to cover the Pareto front uniformly. Generally, the success rate of yielding the sets of noninferior solutions is very high, and the developed algorithms are easily usable for obtaining technically valuable results. Moreover, suggested graphical technique consisting in up to quasi four-dimensional multiplots and aggregate ones enables easier assessments of available trade-offs. The method was successfully tested on more examples, and three of them were presented. The first demonstrates a sophisticated optimization of the highly nonlinear circuit in the time domain, the second performs a sophisticated four-dimensional nonlinear optimization of a video amplifier, and the third represents a two-dimensional design of a low-noise amplifier. Finally, the necessity of a combination of a metaheuristic method with a classical one for solving more complex tasks is discussed.

Acknowledgements

This work has been supported by the Czech Science Foundation under the grant No P102/10/1665 and by the internal grants of the Czech Technical University in Prague SGS 12/151/OHK3/2T/13 and SGS 13/081/OHK3/1T/13. The practical works were performed in laboratories supported by the SIX project; the registration number CZ.1.05/2.1.00/03.0072, the operational program Research and Development for Innovation.

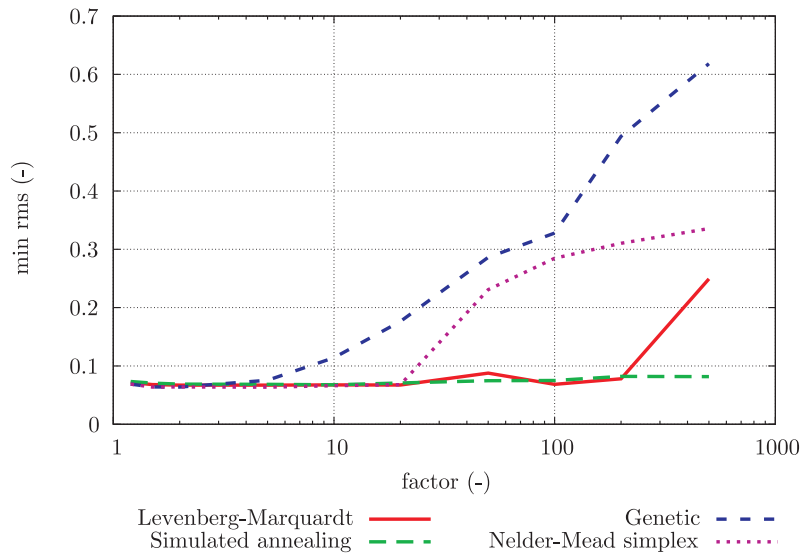


Fig. 21. Minimal root-mean-square values obtained for various widths of parameter space during optimization for chosen operating point.

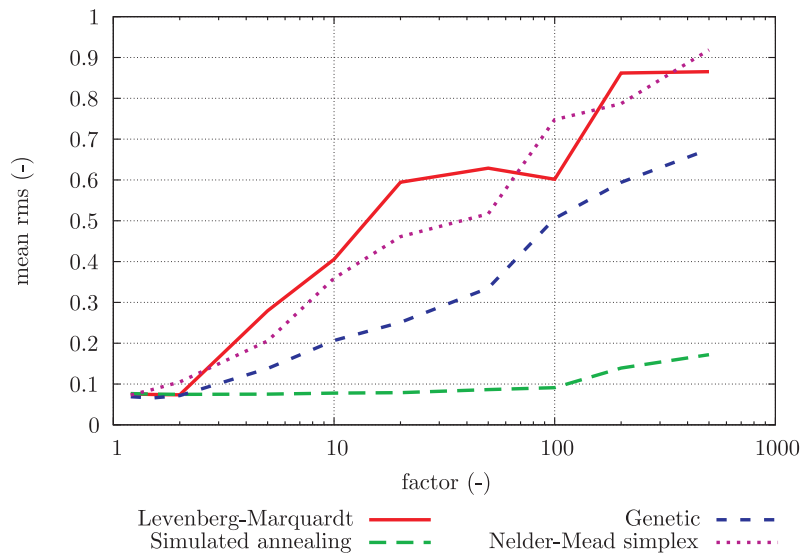


Fig. 22. Mean root-mean-square values obtained for various widths of parameter space during optimization for chosen operating point.

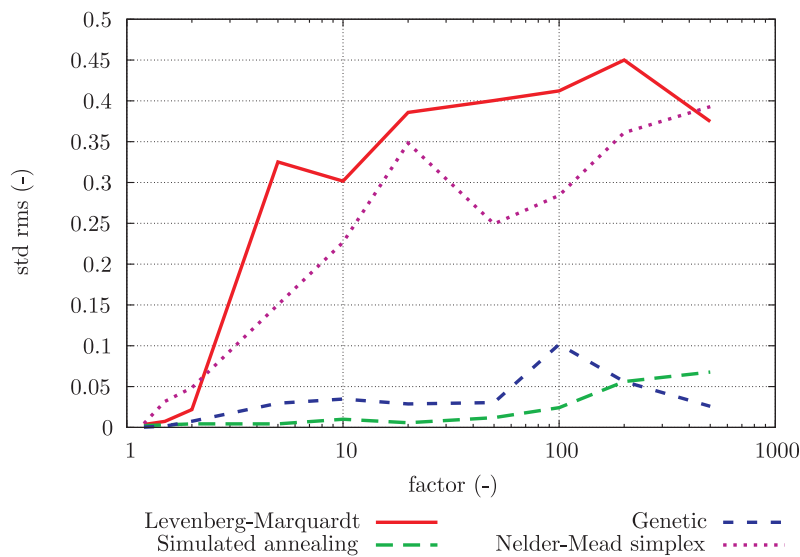


Fig. 23. Standard root-mean-square values obtained for various widths of parameter space during optimization for chosen operating point.

References

- [1] MIETTINEN, K. K. *Nonlinear Multiobjective Optimization*. Boston (MA, USA): Kluwer Academic Publishers, 1998.
- [2] KOLO, B. *Single & Multiple Objective Optimization*. Weatherford (OK, USA): Weatherford Press, 2010.
- [3] COLLETTE, Y., SIARRY, P. *Multiobjective Optimization (Principles and Case Studies)*, 2nd ed. Berlin (Germany): Springer, 2004.
- [4] SHORBAGY, M., MOUSA, A. A. A., FATHI, W. *Hybrid Particle Swarm Algorithm for Multiobjective Optimization (Integrating Particle Swarm Optimization with Genetic Algorithms for Multiobjective Optimization)*. Saarbrücken (Germany): LAP (Lambert Academic Publishing), 2011.
- [5] BRUSCHI, P., NAVARRINI, D., TARROBOIRO, G., RAFFA, G. Acomputationally efficient technique for the optimization of two stage CMOS operational amplifiers. In *Proceedings of the 16th European Conference on Circuit Theory and Design*. Cracow (Poland), 2003, p. 305 - 308.
- [6] MÍČHAL, J., DOBEŠ, J. Electronic circuit design using multiobjective optimization. In *Proceedings of the 50th IEEE Midwest Symposium on Circuits and Systems*. Montréal (Canada), 2007, p. 734 - 737.
- [7] COLEMAN, T. F., ZHANG, Y. *Optimization Toolbox 4 – User's Guide*. Natick (MA, USA): The MathWorks, Inc., 2008.
- [8] MOOSAVIAN, S. A. A., GHAFARI, A., SALIMI, A., ABDI, N. Non-linear multiobjective optimization for control of hydropower plants network. In *Proceedings of the IEEE International Conference on Advanced Intelligent Mechatronics*. Xi'an (China), 2008, p. 1278 - 1283.
- [9] DOBEŠ, J., BIOLKOVÁ, V. Reliable and efficient procedure for steady-state analysis of nonautonomous and autonomous systems. *Radioengineering*, 2012, vol. 21, no. 1, p. 374 - 385.
- [10] DOBEŠ, J. Advanced types of the sensitivity analysis in frequency and time domains. *AEÜ – International Journal of Electronics and Communications*, 2009, vol. 63, no. 1, p. 52 - 64.
- [11] ALLSTOT, D., CHOI, K., PARK, J. *Parasitic-Aware Optimization of CMOS RF Circuits*. New York (USA): Kluwer Academic Publishers, 2003.
- [12] HOROWITZ, P., HILL, W. *The Art of Electronics*. Cambridge (UK): Cambridge University Press, 1989.
- [13] DOBEŠ, J., MÍČHAL, J., PAŇKO, V., POSPÍŠIL, L. Reliable procedure for electrical characterization of MOS-based devices, *Solid-State Electronics*, 2010, vol. 54, no. 10, p. 1173 - 1184.
- [14] TLELO-CAUATLE, E., GUERRA-GÓMEZ, I., DE LA FRAGA, L. G., FLORES-BECERRA, G., POLANCO-MARTAGÓN, S., FAKHFAKH, M., REYES-GARCÍA, C. A., RODRÍGUEZ-GÓMEZ, G., REYES-SALGADO, G. Evolutionary algorithms in the optimal sizing of analog circuits. *Intelligent Computational Optimization in Engineering, Studies in Computational Intelligence*. Berlin (Germany): Springer, 2011, vol. 366, p. 109 - 138.
- [15] FAKHFAKH, M., SALLEM, A., BOUGHARIOU, M., BENNOUR, S., BRADAI, E., GADDOUR, E., LOULOU, M. Analogue circuit optimization through a hybrid approach. *Intelligent Computational Optimization in Engineering, Studies in Computational Intelligence*. Berlin (Germany): Springer, 2011, vol. 366, p. 297 - 327.
- [16] MOUSA, A. A. A. *Study on Multiobjective Optimization Using Improved Genetic Algorithm (Methodology and Application)*. Saarbrücken (Germany): LAP (Lambert Academic Publishing), 2011.
- [17] MIYAZAKI, R., HAMADA, N., NAGATA, Y., ONO, I. A new Pareto frontier covering strategy in FS-MOGA for multi-objective function optimization. In *Proceedings of the 6th International Conference on Soft Computing and Intelligent Systems/13th International Symposium on Advanced Intelligent Systems*. Kobe (Japan), 2012, p. 1888 - 1893.
- [18] HIRANO, H., YOSHIKAWA, T. A study on two-step search using global-best in PSO for multi-objective optimization problems. In *Proceedings of the 6th International Conference on Soft Computing and Intelligent Systems/13th International Symposium on Advanced Intelligent Systems*. Kobe (Japan), 2012, p. 1894 - 1897.
- [19] CHIBA, K. Performance comparison of evolutionary algorithms applied to hybrid rocket problem. In *Proceedings of the 6th International Conference on Soft Computing and Intelligent Systems/13th International Symposium on Advanced Intelligent Systems*. Kobe (Japan), 2012, p. 1673 - 1678.
- [20] PAPA, D. A., MARKOV, I. L. *Multi-Objective Optimization in Physical Synthesis of Integrated Circuits*. New York (NY, USA): Springer, 2013.
- [21] ZHOU, Y., GAD, E., NAKHLA, M. S., ACHAR, R. Structural characterization and efficient implementation technique for A-stable high-order integration methods. *IEEE Transactions on Computer-Aided Design of Integrated Circuits and Systems*, 2012, vol. 31, no. 1, p. 101 - 108.
- [22] DOBEŠ, J., GRÁBNER, M. Novel HEMT models with improved higher-order derivatives and extracting their parameters using multi-bias S-parameters. In *Proceedings of the 33rd IEEE Compound Semiconductor Integrated Circuit Symposium*. Waikoloa, Big Island (HI, USA), 2011, p. 189 - 192.

About Authors...

Josef DOBEŠ received the Ph.D. degree in microelectronics at the Czech Technical University in Prague in 1986. From 1986 to 1992, he was a researcher of the TESLA Research Institute, where he performed analyses on algorithms for CMOS Technology Simulators. Currently, he works at the Department of Radio Electronics of the Czech Technical University in Prague. His research interests include the physical modeling of radio electronic circuit elements, especially RF and microwave transistors and transmission lines, creating or improving special algorithms for the circuit analysis and optimization, such as time- and frequency-domain sensitivity, poles-zeros or steady-state analyses, and creating a comprehensive CAD tool for the analysis and optimization of RF and microwave circuits.

Jan MÍČHAL received his M.Sc. degree in electrical engineering from the Czech Technical University in Prague in 1993. He received the Ph.D. degree in radio engineering at the Czech Technical University in Prague in 1986. Currently, he works as a researcher at the Division of Integrated Circuit Design of CertiCon Corporation. His research interests mainly consist in the numerical methods for RF circuit analysis and synthesis, especially optimization methods, and practical designing the RF circuits.

Viera BIOLKOVÁ received her MSc degree in electrical engineering from the Brno University of Technology, Czech Republic, in 1983. She joined the Department of Radio Electronics in 1985 and is currently working as a research assistant at the Department of Radio Electronics, Brno University of Technology (BUT), Czech Republic. Her research and educational interests include signal theory, analogue signal processing and digital electronics.